Experimental and theoretical analysis of collective effects in electron-impact ionization phenomena

F. Giammanco
Dipartimento di Fisica, Università di Pisa, Piazza Torricelli 2, 56126 Pisa, Italy

G. Arena, R. Bruzzese, and N. Spinelli
Dipartimento di Scienze Fisiche, Università di Napoli, Padiglione 20, Mostra d'Oltremare, 80125, Napoli, Italy
(Received 2 February 1989; revised manuscript received 24 October 1989)

An experimental analysis of collective effects, depending on the electron-ion mutual interactions, which occur during the ionization of a gas jet by impact with an incident monochromatic pulsed electron beam, is presented. The dependences on the gas pressure of the transmitted current and of the ion yields show a marked deviation, in the same range of gas pressure, i.e., of produced charges, from the expected behavior in the absence of interactions between incident and produced charges. The phenomenon is described by an approximate solution of the two-fluid equation system that takes into account the transient phase, during the impact ionization, and the symmetry of the experiment. The theoretical model well explains the observed dependences.

I. INTRODUCTION

The importance of collective effects, depending on the electron-ion mutual interaction, in experiments involving the production and collection of charged particles, e.g., laser multiphoton ionization (MPI), has been recently highlighted and analyzed.[1-3] In particular, a great deal of attention has been directed to the perturbative influence of the above phenomena during the collection phase of the initially produced charges. It has been pointed out[1,4] that the time-space behavior of charges, as produced in typical experiments of atomic physics,[5-13] could be strongly affected by the appearance of a macroscopic electric field, due to the different mobilities of electrons and ions. Hence, the noticeable modifications of the parameters (number density, kinetic energy of electrons, velocity distribution, and so on) of the initially produced charges, induce relevant deviations of the observed dependences on the experimental parameters (laser power, external field, neutral density) from those expected as a consequence of the selected laser-matter interaction. Although many authors[5-13] concerned with different fields of investigations and applications introduced the so-called "space-charge" effect as a possible explanation of the observed "anomalous" dependences on the laser power; nevertheless, no experimental work was especially performed to carry out a detailed analysis of the collective plasma phenomena and their range of influence.

The experiment of Ref. 2, concerning the three-photon ionization of a Na beam in a range of the experimental parameters common to most MPI experiments, was specifically carried out in order to analyze the main features of the charge evolution. The influence of the self-generated electric field was investigated through an analysis of the electron current and ion yield dependences on the externally applied electric field, laser power, and focusing conditions, at different initial gas densities.

The theoretical model, based on the three-dimensional fluid description of coupled motion[3] of electrons and ions and also including the production phase during the laser-gas interaction time, represents an extension of the analytic method of solution presented in Ref. 1, and is able to give a quantitative description of the observed dependences.

Collective effects were also observed in completely different experimental conditions, namely, during the pulsed injection of a nonrelativistic (on the order of keV energies) electron beam in a low density (10^{-5} Torr) gas.[14,15] In this case, a transient stage precedes the steady state, where the produced charges are completely neutralized. During this transient stage there is a progressive increase of the ion density in the gas, as ions are produced in electron-atom collisions. In the time interval characterizing this stage there is a monotonic transition from a completely unneutralized beam, which is therefore highly divergent in absence of external fields, to a steady-state beam. What is experimentally observed is a clearly expressed dynamic ion focusing of the electron beam. This focusing was described[14] as an increase of the axial beam current density to the point at which, some time after the beginning of beam injection into the gas, this current density was far greater than the steady-state current density of the beam.

In this paper the observation of relevant collective effects in the process of electron-impact (EI) ionization of low-density atomic and molecular gases (pressure 10^{-6}–10^{-4} Torr) is reported. Collective effects are reported in the experimental conditions characterizing EI ionization phenomena. In particular, we have observed a focusing ion effect on the electronic beam very similar to that reported in Ref. 14, but at electron energies (≈ 40 eV) about 100 times smaller than those characterizing the beams of Refs. 14 and 15 (≈ 1 keV), and with an electron-beam–gas interaction time (≈ 10 nsec) that does not allow the establishment of a steady-state condition.

This focusing effect results, in the present case, in an increase of the axial current measured by an electron detector, whose radius is smaller than the radial width of the unperturbed electron beam, which monitors the electron-beam current after it has passed through the target gas.

The observed effect shows a strong dependence on the gas pressure, i.e., on the degree of ionization produced. Actually, the peak and the total charge of the electron current exhibit a sudden growth in a very small range of pressure variation and subsequently the behavior is quite flat, except for a nonregular modulation.

The total ion count rate exhibits a change in the slope in correspondence of the same range of pressure. Moreover, the shape of the peaks in the time-of-flight (TOF) spectrum of the produced ions changes as a function of the gas pressure, showing a growing tail in the region of increasing time of flight.

By adapting the theoretical approach described in Refs. 1 and 3, in order to include the specific features of the experiment, an analysis of the phenomena has been carried out, as well as a detailed comparison with the experimental results. The analytic method, although previously described,[1,3] is recalled with the aim of clarifying the modifications introduced in order to take into account the involved physical phenomena (Sec. III).

II. EXPERIMENTAL RESULTS

Figure 1 shows a schematic view of the experimental setup. This apparatus is similar to that used in previous experiments[16,17] and, thus, only a short description is given here.

The time-of-flight ion spectrometer is made up of a 40-cm-long drift tube. The ions are accelerated at the entrance of the TOF tube by three gaps, where three different electric fields are applied. The electron beam is produced by a pulsed electron gun, which includes an indirectly heated oxide cathode and two electrostatic lenses. The mean kinetic energy of the electrons is 37.5±0.2 eV. The value of the current peak is 100 nA, with a pulse duration of 10 nsec at a repetition frequency of 4 kHz. The radial width of the beam in the focal region that corresponds to the interaction region is 0.1 cm. The electron beam is monitored by an electron multiplier whose first dinode is positioned 2 cm from the interaction region and whose diameter is 0.25 cm. The electron current signal is fed into a fast (< 1 nsec rise time) oscilloscope (Tektronix 7844) equipped with a digitizing camera (Tektronix, mod. DCS 01) which is interfaced with a personal computer for data storage and analysis.

The gas target, a mixture of Ar and CO_2, is introduced in the ion source through a 10-μm-diam stainless-steel needle injector fed by a variable, programmable, self-controlling leak. The whole apparatus is contained in a stainless-steel chamber, with a residual gas pressure (after baking at 200–300 °C) of about 10^{-8} Torr. The overall working pressure in the vacuum vessel during the measurements ranges between 10^{-6} and 10^{-4} Torr, while the local pressure, just above the needle injector, is about 100 times higher. This factor was estimated by measuring in previous MPI experiments with visible laser light the ionization rate both with and without the needle injector, in the same experimental apparatus. We have corrected the value obtained in the case of laser ionization for the different interaction volume characterizing the electron-beam ionization experiment. The final estimation of a factor of 100 can be taken with a confidence of 20%. Thus, although we have reported on the horizontal axes of Figs. 2–4 only the values of the overall gas pressure in the vacuum chamber, both for cases (*a*) and (*b*), the value of 100 (±20%) has to be used as a scale factor for obtaining the actual local pressure, characterizing the points of the curves labeled (*a*) in the above figures.

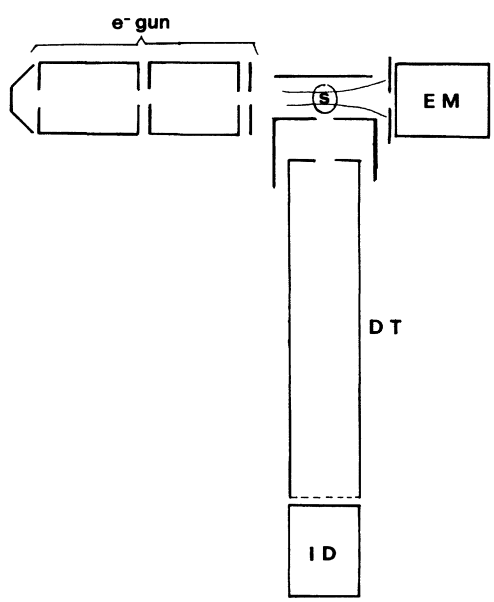

FIG. 1. Schematic view of the experimental setup. *e*-gun, pulsed electron gun; *S*, ion source region; EM, electron multiplier; DT, drift tube; ID, ion detector.

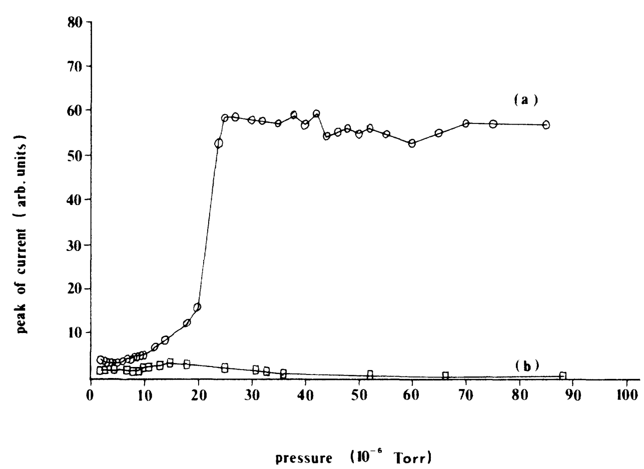

FIG. 2. Peak of the transmitted electron-beam current as a function of the overall gas pressure in the vacuum chamber. Curve (*a*), gas injected into the vacuum chamber through the needle injector; curve (*b*), no needle injector. Note that, as discussed in the text, a multiplicative scale factor of 100±20 has to be used on the horizontal axis for obtaining the actual pressure characterizing the points of curve (*a*).

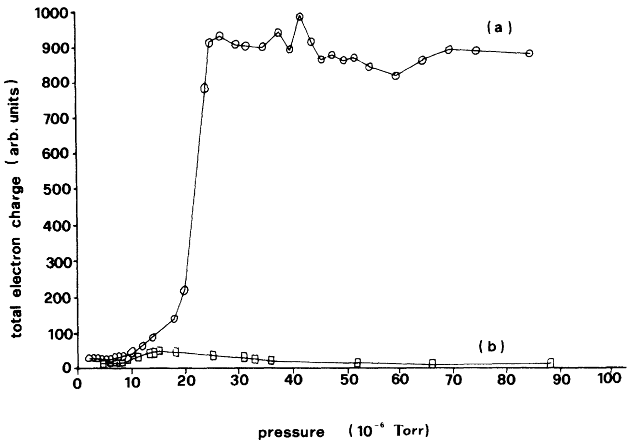

FIG. 3. Total collected charge of the electron-beam pulse as a function of the gas pressure. Cases (*a*) and (*b*) as in Fig. 2.

The ion accelerating electric field ($E=100$ V/cm) is switched on as soon as the electron pulse has left the ion source region (*S*). At the end of the field-free drift tube the ions are detected by a windowless focused electron multiplier (EM). The ions are identified by measuring their time of flight. For the selected gas mixture the TOF's of the different ionic species range between 4 and 5 μsec. The electric signal from the ion detector is fed into an electronic circuit whose features are described in Refs. 16 and 17. The overall time resolution of the ion spectrometer is better than 1 nsec.

The experimental results proposed here deal with the characterization of the focusing effects as observed in the propagation of the incident beam and in the collection of the ion yields. Particularly, the dependences of the electron current and total ion count rate on the gas pressure, i.e., on the produced charge density, display the most interesting features characterizing our experiment. Moreover, the explanation of the observed dependences constitutes a first suitable test for a theoretical model whose aim is a detailed quantitative description of the processes occurring during the interaction.

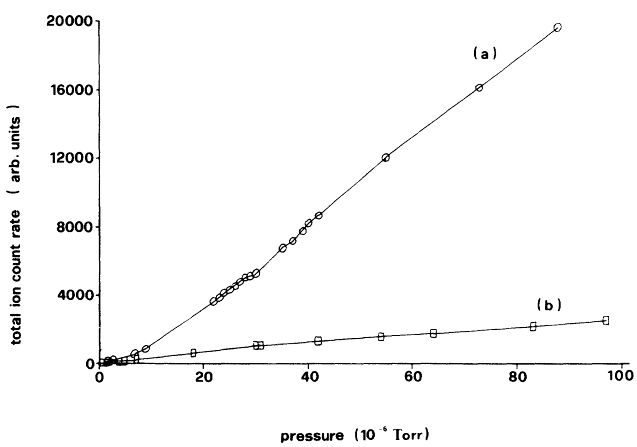

FIG. 4. Total ion count rate as a function of the gas pressure. Cases (*a*) and (*b*) as in Figs. 2 and 3.

Figure 2, curve (*a*), shows the behavior of the peak of the transmitted current as a function of the gas-pressure mean value in the chamber when the gas mixture is introduced in the vacuum chamber through the needle injector. The axial current is insensitive to pressure variations up to about 10^{-5} Torr, corresponding to 10^{-3} Torr just above the needle injector. Above this value the linear growth between $\approx 10^{-5}$ and $\approx 2\times10^{-5}$ Torr is followed by a sudden dramatic increase, in correspondence with a very small pressure variation, that subsequently leads to a plateau region, where the peak value is about ten times greater than the unperturbed one. A further increase of pressure above $\approx 2.5\times10^{-5}$ Torr introduces only a small modulation around the maximum achieved value. The dependence of the total collected charge of the electron pulse current exhibits the same behavior [Fig. 3 curve (*a*)]. In this case the maximum ratio between the total charge of the unperturbed current and the plateau value is about 30.

Figure 2, curve (*b*), and Fig. 3, curve (*b*), represent the experimental results obtained when the gas mixture is introduced in the vacuum chamber without a needle injector (uniform gas pressure). In this case the focusing effect is not observed. Recalling that the local pressure in the case of gas injected by the needle is 100 times the mean pressure, it is evident that the density of produced charges is strongly reduced. Moreover, as will be seen better in Sec. IV, in this case the dimension of the interaction zone is only determined by the cross section of the electron beam. This leads to a smoother charge-density gradient than in the previous measurements.

The appearance of the focusing electric field depends on the rate of charge separation during the interaction time and, particularly, on the electron mobility, which is a function of the density gradient (see Sec. III). Hence, in the case of uniform gas pressure, the absence of focusing effects is ascribed not only to the low level of produced charge density, but mostly to the strong decreasing of its gradient.

Figure 4, curve (*a*), shows the dependence of the total ion count rate on the gas pressure as observed when the gas mixture is injected through the needle. As a comparison, the same measurements, performed under conditions of uniform gas pressure, are represented by Fig.

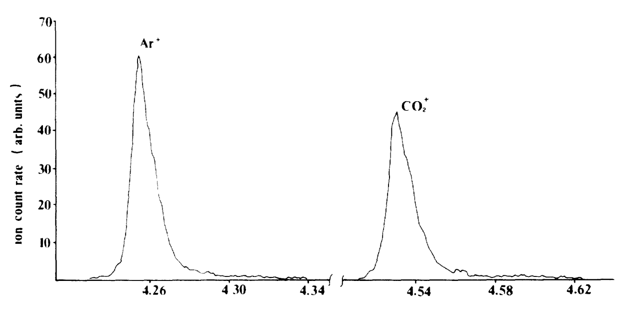

FIG. 5. TOF ion mass spectrum obtained with the gas injected through the needle and with a mean pressure of 3.8×10^{-6} Torr.

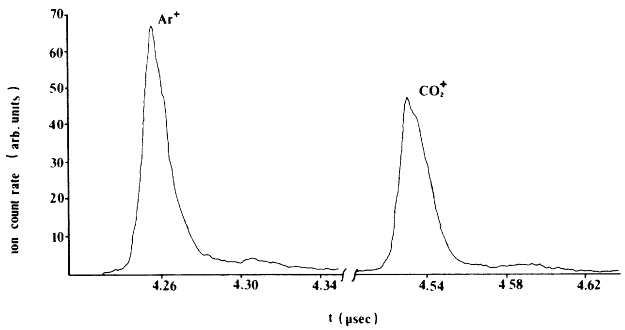

FIG. 6. TOF ion mass spectrum with the same conditions of Fig. 5 but with a mean gas pressure of 3.3×10^{-5} Torr.

4(*b*). Up to $\approx10^{-5}$ Torr both curves overlap. As the pressure is increased, in the same region where the sudden growth of the electron current is observed, the ion dependence, although still linear, exhibits a relevant change in slope, whereas no modifications occur in the case of uniform pressure. A more detailed inspection of Fig. 4 shows a sort of modulation of the slope in the region between $\approx10^{-5}$ and $\approx4\times10^{-5}$ Torr in correspondence with the modulation of the electron current.

The TOF spectrum of the ions also shows interesting differences if observed at different gas pressures. Whereas in the pressure range where no focusing effects occur the spectrum is constituted by single well-defined peaks (Fig. 5), on the contrary, the sharpness of the peaks is reduced as the pressure increases. Moreover, relevant tails in the region of longer TOF's are observed (see Fig. 6).

In order to better show these differences, we present in Fig. 7 what is obtained by subtracting the spectrum of Fig. 5 from that of Fig. 6. In Fig. 7, the vertical arrows indicate the location of the maxima of Ar^+ and $CO_2{}^+$ peaks of Figs. 5 and 6. The arrows correspond to zero counts because both Ar^+ and $CO_2{}^+$ peaks have been normalized to the same values. The spectrum of Fig. 7 highlights the presence of both a relevant and asymmetric broadening of the peaks and of considerable tails in the region of longer TOF's.

These last results support the interpretation based on

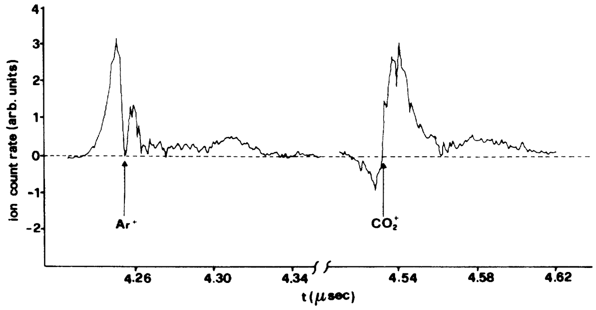

FIG. 7. TOF spectrum obtained by subtracting the spectrum of Fig. 5 from that of Fig. 6. The vertical arrows indicate the locations of the maxima of the Ar^+ and $CO_2{}^+$ peaks of Figs. 5 and 6.

the collective plasma effects due to the secondary produced charges. The presence in the TOF ion spectrum of the tails of Fig. 6 resembles those observed in Ref. 2, where a Na beam was ionized by a laser pulse and the ions were collected by an electric field of about 14 V/cm. As in the case of Ref. 2, the observed behavior can be ascribed to the screening of the external field by the self-generated electric field due to the different mobility of charges.

III. THEORETICAL MODEL

The observed surprising behavior of both electron transmitted current and ion total yield as a function of the gas pressure can be analyzed by using a theoretical approach similar to that used in Refs. 1 and 3, provided some peculiar features of this experiment are included in the model. In fact, the main features of produced charges are quite similar to those observed in typical experiments of multiphoton ionization, above-threshold ionization, and so on. As previously pointed out,[1,3] the fluid approximation constitutes a suitable approach to describe the time-space evolution of charges, in spite of the fact that the velocity distribution function is, in general, quite far from the equilibrium Maxwell distribution. In fact, the fluid scheme, derived from the Boltzmann transport equation as momenta of different order averaged over the velocity distribution function, holds true, providing that the averaged particle velocity is equal to zero. Thus an isotropic velocity distribution, regardless of its shape, is sufficient to make the fluid approach valid. The basic equations describe the time-space evolution of the fluid mean quantities (velocity, density, and energy) referred to the laboratory frame. It turns out that they are functions of coordinates and of time. The fluid velocity represents the common component of collective motion, whereas the temperature is related to the mean kinetic energy of random motion of the particles. In the case of isothermal expansion in a vacuum, two partial differential equations, for fluid velocity and density, are sufficient to characterize the evolution, namely, motion and continuity equations.[17] For each species involved in the present experiment, the basic equations are given by

$$\frac{\partial \mathbf{v}_j}{\partial t}+(\mathbf{v}_j\cdot\nabla)\mathbf{v}_j=\frac{e_j}{m_j}(\mathbf{E}_0+\mathbf{E}_r)-\frac{2E_j}{m_j}\nabla\ln(n_j)\ , \quad (1)$$

$$\frac{\partial n_j}{\partial t}+\nabla\cdot(n_j\mathbf{v}_j)=S_j\ , \quad (2)$$

where $\mathbf{v}_j$, e_j, m_j, and n_j are the collective velocity, charge, mass, and density of the selected species. $\mathbf{E}_0$ represents the external electric field. The subscript j refers to the incident electrons (p) and to the secondary electrons and ions ($j=e,i$) produced by impact ionization, respectively. S_j represents the source term responsible for the growth of ionization ($S_p=0$ for the incident electron beam). Since the temperature is, in the present experimental conditions, a meaningless quantity in front of the very long electron-electron and electron-ion equipartition time,[18] in Eq. (1) we have introduced the term E_j, which is related to the mean energy of random motion in place of the temperature, as in the case of charges produced by multiphoton ionization.[1,3] Thus, in the case of incident electrons, E_j is equal to the thermal spread (E_B) of the beam. In the case of secondary electrons and ions, E_j is equal to the mean kinetic energy of ejected electrons (E_{se}), and to the gas kinetic energy (E_{si}), respectively.

In Eq. (1) $\mathbf{E}_r$ is the self-generated electric field given by the Poisson equation

$$\nabla \cdot \mathbf{E}_r = 4\pi e (n_i - n_e - n_p) . \quad (3)$$

Thus Eqs. (1) and (2) for each species are coupled together by the internal field.

In the present experiment owing to the short ionization time (≈ 10 nsec) and the very small interaction volume that implies strong density gradients, the complete system cannot be simplified by using the usual plasma physics approximations, based on local neutrality and small time-space variation of macroscopic quantities (charge density, self-generated field, and so on).

An approximate evaluation of the term depending on the density gradient in Eq. (1) shows that the dimensions of the interaction zone play a crucial role in the observed focusing phenomena, as stated by the experimental results of Sec. II, and by comparison with those of Refs. 14 and 15. In fact, produced electrons initially leave the interaction volume, whose width is d, as an effect of their random velocity in a characteristic time $\tau_{se} = (m/4E_{se})^{1/2} d$, the external field being zero during the interaction time. A positive internal field, due to the ions at rest, stops the decrease of electron density and reverses the electron motion. Therefore, incident and produced electrons are focused and their local density overcomes the ionic one, because of the excess of negative charges due to the incident electron beam, in such a way that ions too begin to be focused. The further ion motion in the external field is then affected by the preceding coupled interaction among incident electrons and produced electrons and ions.

First of all, the efficiency of the process depends on the time scale of electron expansion compared with the duration of the interaction, in the present experiment ≈ 10 nsec. In the case of gas injected by needle ($d \approx 0.01$ cm), $E_{se} \approx 2$ eV, and thus $\tau_{se} \approx 0.1$ nsec, whereas in presence of uniform gas pressure $\tau_{se} \approx 4$ nsec, with a cross section of the electron beam of ≈ 0.4 cm. Moreover, the growth of the restoring ion field depends on the rate of produced charges, i.e., on the intensity of the incident current and of the gas pressure. Finally, the net excess of negative charges, depending on the intensity of the incident current, is responsible for the ion focusing.

If the spatial profile of involved species is approximated by a Gaussian-shaped profile, it is demonstrated in Ref. 1 that the uncoupled motion of each species, i.e., with $E_r = 0$, is still represented by a Gaussian-shaped profile, whose width is a function of time and whose maximum translates according to the single-particle motion in an external field E_0. Thus the one-dimensional time-space evolution of each density profile in the presence of a uniform electric field E_0 along the x axis may be expressed as

$$n_j(x,t) = n_0 [f(t)]_j^{1/2} \exp[-f_j(t)(x - x_j^s)^2/d^2] \quad (j = i,e,p) , \quad (4)$$

where d and n_0 represent the initial charge distribution width and density, respectively, while $x_j^s = \int v_j^s dt$, with $Dv_j^s = e_j E_0(t)/m_j$, represents the electron or ion single-particle motion in the external electric field, D being the total derivative. The continuity equation provides the functional dependence of the fluid mean velocities on n_j and, thus, on the $f_j(t)$ functions appearing in Eq. (4), namely, $v_j = 0.5(x_j^s - x)\{D \ln[f_j(t)]\}$. The functions $f_j(t)$ satisfy the initial conditions $f_j(t=0) = 1$, and $Df_j(t)|_{t=0} = 0$. A second-order differential equation describing the $f_j(t)$ time evolution is derived from the motion equation by replacing the $f_j(t)$ functional dependencies for both mean velocity and n_j, and by equating the terms with the same power dependence on the spatial coordinates. Owing to the independence of motion along the axes, the three-dimensional motion is represented by a product of three Gaussian profiles with different initial widths, depending on the symmetry of the charges production. Thus the time evolution of $f_j(t)$ along any axes depends on the initial width. Owing to the structure of the basic equations (1) and (2), terms in the form $G(t) + F(t)\mathbf{r}$, where $\mathbf{r} = (x,y,z)$, can be included, only requiring modification in the differential equations for $f_j(t)$ and the single-particle-like ones. In general, the inclusion of the internal field E_r and of the source terms S_j makes the previous solution scheme invalid. Nevertheless, under suitable hypothesis both terms can be reduced to a form in which the basic solution scheme still holds true.

The Poisson equation is linearized around the coordinates of the single-particle motion for the electrons and ions, i.e., around the top of the Gaussian profiles. As an example of the technique, in the one-dimensional case and for two generic electron and ion species, integrating between $-\infty$ and x, and introducing the variable change $\varepsilon_j = f_j^{1/2}(x_j^s - x)/d$, where the index j refers to both the species, the internal field is given by

$$E_r(x,t) = 4\pi e d n_0 \int_{\varepsilon_i}^{\varepsilon_e} e^{-\varepsilon^2} d\varepsilon , \quad (5)$$

where the subscripts i and e refer to ions and electrons, respectively.

By series integration and retaining the first term only, one immediately obtains

$$E_r(x,t) = 4\pi e n_0 [f_i^{1/2}(x - x_i^s) - f_e^{1/2}(x - x_e^s)] . \quad (6)$$

Equation (6) is valid insofar as the second term of the series development is negligible. This allows one to obtain the spatial interval of validity of the previous solution from the condition

$$\varepsilon_e - \varepsilon_i \ge (\varepsilon_e^3 - \varepsilon_i^3)/3 . \quad (7)$$

In the form of Eq. (6), the internal field can be introduced in the basic system of Eqs. (1) and (2); and by equating terms with the same power of x, the new differential equations for $f_j(t)$ and $x_j^s(t)$ are immediately obtained.

When the condition of Eq. (7) is not met, the motion is still represented by a Gaussian profile freely expanding, i.e., with $E_r=0$, weighted by the total number of particles able to overcome the internal field, namely,

$$n_f=k(t)[f(t)]^{1/2}\exp[-f(t)(x/d)^2] .$$

$k(t)$ is given by the mass conservation, i.e.,

$$n_0 2\int_0^{\varepsilon^*} e^{-\varepsilon^2}d\varepsilon+k(t)2\int_{\varepsilon^*}^{\infty} e^{-\varepsilon^2}d\varepsilon=\sqrt{\pi}\, dn_0 , \qquad (8)$$

where ε^* is a value that satisfies condition (7). The first integral is calculated by introducing the value of $f(t)$ given by the coupled system, whereas in the second integral $f(t)$ is the solution with $E_r=0$.

The boundary between coupled and uncoupled zones can be obtained only by an experimental analysis of the ratio between trapped and untrapped particles, as in Refs. 2 and 3, since this value depends strongly on the experimental conditions. Thus, in the present experiment, additional experimental information is required in order to compare predicted and observed ion TOF distribution.

As in the case of freely expanding motion, the three-dimensional extension is easy, and the internal field depends on the square root of the product of three $f_j(t)$ functions. It follows that the internal field couples the motion along any axis for each species, and the motion of each species together.

The production term S_j can be introduced in the previous scheme at a degree of approximation of the same order of that used in linearizing the Poisson equation. Generally speaking, if the time scale of expansion greatly differs from the production time, the term representing the flux of particles $[\nabla\cdot(n\mathbf{v})]$ can be neglected. In this case, the continuity equation reduces to the usual rate equation admitting separation of variables, if the production term can be expressed as a product of two separate functions of the spatial coordinates and time. Under the conditions of the present experiment during the interaction time between the gas and the electron beam (10 nsec), ions are at rest. In fact, the external field is switched on after the end of the interaction, and the time scale of thermal expansion (τ_i) is about 0.1 μsec. Therefore, it is sufficient to replace n_0 in Eq. (4) by the solution $g(t)$ of the rate equation

$$\frac{dg(t)}{dt}=\langle a\rangle n_p[N-g(t)] . \qquad (9)$$

In Eq. (9) N represents the unperturbed gas density, n_p the electron-beam density, and $\langle a\rangle$ (cm^3/sec) the ionization cross section averaged over the velocity distribution function. It has been also assumed that only ions and molecules in the fundamental state are present in the gas.

Owing to the different time scale of expansion $[\tau_{se}=(m/4E_{se})^{1/2}d\approx 0.1$ nsec], in principle, the behavior of electrons produced during the interaction cannot be described in as simple a way as that of ions, if detailed information of the time-space profile is required. Nevertheless, it is demonstrated in Ref. 3 that, in the case of τ_{se} much less than the interaction time, the electron time-space profile is similar to the ionic one.

The geometrical characteristics of the experiment lead to an important simplification as to the number of differential equations to be solved. The incident beam is described in a cylindrical symmetry around the propagation axis (x) by radial and longitudinal Gaussian profiles, whose widths are d_r and d_x, respectively. It is a reasonable approximation to assume a spherical expansion of the produced charges. Thus the complete scheme includes a system of four differential equations, of which two refer to the longitudinal and radial $f(t)$ functions of the beam [$f_{px}(t)$ and $f_{pr}(t)$, respectively], and the other two to both secondary ion and electron $f(t)$ functions [$f_{si}(t)$ and $f_{se}(t)$, respectively]. The contribution coming from the region of free expansion does not affect the growth of the transmitted current, whereas it is important if details of the ion time behavior are required. In fact, the free expansion does not depend on the produced charge density ($E_r=0$). An additional contribution comes from momentum-exchange collisions with neutral particles, whose frequency could be comparable with the time scale of the interaction.[1] Nevertheless, owing to the range of pressure variation, this contribution can be neglected.

The differential equations for the $f_j(t)$ functions, during the interaction time ($E_0=0$) are given by

$$D^2 f_j=\frac{3}{2}\frac{(Df_j)^2}{f_j}-2(f_j/\tau_j)^2+C(g(t),f_i,f_e,f_{px},f_{pr}) , \qquad (10)$$

where τ_j is the characteristic time constant of free expansion due to the density gradient of the involved species, given, respectively, by

$$\tau_{px}^2=\frac{m_e d_x^2}{4E_B},\quad \tau_{pr}^2=\frac{m_e d_r^2}{4E_B},\quad \tau_{sj}^2=\frac{m_e d_s^2}{4E_{sj}} , \qquad (11)$$

where E_B is the energy spread of the electron beam, d_x and d_r its longitudinal and radial widths, respectively, and $j=i,e$ for secondary charges. E_{se} represents the mean energy of the secondary electrons, produced in an almost spherical interaction volume of radius d_s, whereas E_{si} is given by the gas temperature. The coupling term $C(g(t),f_i,f_e,f_{px},f_{pr})$, due to the internal field, is for each species given by

$$\frac{2}{3}\left[\frac{4\pi e^2}{m_e}\right]\{Ng(t)f_{si}^{3/2}-[Ng(t)f_{se}^{3/2}+n_p f_{px}^{1/2}f_{pr}]\}f_{px} ,$$

$$\frac{2}{3}\left[\frac{4\pi e^2}{m_e}\right]\{Ng(t)f_{si}^{3/2}-[Ng(t)f_{se}^{3/2}-n_p f_{px}^{1/2}f_{pr}]\}f_{pr} , \qquad (12)$$

$$\pm\frac{2}{3}\left[\frac{4\pi e^2}{m_e}\right]\{Ng(t)f_{si}^{3/2}-[Ng(t)f_{se}^{3/2}+n_p f_{px}^{1/2}f_{pr}]\}f_{sj} .$$

The last term refers to secondary charges and the upper sign to the electrons. The initial conditions are, of course, $f_j(t)=0$ and $Df_j(t)|_{t=0}=0$. The Poisson equation now involves also the primary electrons, whose contribution is given by $n_p f_{px}^{1/2}f_{pr}$. The function $g(t)$ is obtained as the solution of Eq. (9), assuming a constant density of the primary electrons during the interaction and normalizing to the gas density N, i.e.,

$$g(t)=(1-e^{-\langle a\rangle n_p t}) .$$

The coupling terms given by Eqs. (12) are effective during the interaction time that depends on the duration of the electron beam pulse and on its velocity v_0, namely, $t_{\text{int}}=d_x/(f_{px}^{1/2}v_0)$. If the internal field is negligible ($f_{px}=1$) that time is equal to the unperturbed pulse duration ≈ 10 nsec.

For $t>t_{\text{int}}$ the coupling term disappears in the equations relative to the electron beam that freely expands, but with values of the $f(t)$ functions and its derivatives as obtained at the end of the mutual interaction. In the equations for secondary charges, at the end of the interaction, the term depending on n_p vanishes, the function $g(t)$ assumes the constant value $g(t_{\text{int}})$, and two single-particle-like equations must be added to take into account the switching on of the external field, namely,

$$D^2x_j^s=\frac{e_j}{m_j}E_0\pm\tfrac{1}{3}\omega_{pj}^2 f_{\bar{j}}^{3/2}(x_i^s-x_e^s) , \tag{13}$$

where the upper sign refers to electrons; $\omega_{pj}=4\pi e^2Ng(t_{\text{int}})/m_j$ is the plasma frequency. In Eq. (13) the index $\bar{j}$ denotes that if x_j^s refers to ions, $f_{\bar{j}}$ refers to electrons, and vice versa. The initial conditions are $x_j^s(0)=0$ and $Dx_j^s(t)|_{t=0}=0$. The temporal origin of the ion motion is now chosen so as to correspond to the instant of the switching on of the field. The new initial conditions of integration of Eq. (11) for $f_j(t)$ and $Df_j(t)$ are those determined at the end of the interaction with the incident beam.

The total current on the surface of the detector, positioned at a distance $x=A$ from the interaction region ($x=0$), whose radius is R, is obtained by integrating the longitudinal component of the current on the radial variable; this leads to

$$I_{\text{tot}}\propto v_x f_{px}^{1/2}\exp\left[-\frac{f_{px}}{d_x^2}(v_0t-A)^2\right] \times\left[1-\exp\left[-\frac{f_{pr}}{d_r^2}R^2\right]\right] , \tag{14}$$

where v_x is given by $v_x=v_0+0.5(v_0t-A)D\ln(f_{px})$.

The total number of ions on a detector (of diameter R_1), at position A_1, is immediately calculated from

$$N_{i\,\text{tot}}\propto Ng(t_{\text{int}})\int_0^\infty f_{si}^{1/2}\exp\left[-\frac{f_{si}}{d_s^2}(x_{si}-A_1)^2\right] \times\left[1-\exp\left[-\frac{f_{si}}{d_s^2}R_1^2\right]dt\right] . \tag{15}$$

Figure 8 shows, as a function of the gas density, the behavior of the peak of the electron current in typical experimental conditions, that is, $E_B=0.1$ eV, $E_{se}=2$ eV, and $E_{si}=0.1$ eV, and $d_x=2$ cm, $d_r=0.1$ cm, $d_s=0.01$ cm, and $R=0.2$ cm at a position $A=5$ cm. Also, an ionization rate is assumed ($\langle a\rangle n_p$) of 10^4 sec^{-1}, as approximately deduced from the measurements performed at uniform gas pressure [see Fig. 4, curve (*b*)] and a density of incident electrons of 10^9 electrons/cm^3. Figure 9 shows the dependence of the total electron charge on the gas density as obtained by time integration of Eq. (14). Finally, the dependence of the total ion count rate in an external field of ≈ 100 V/cm (Sec. II) on the gas density is shown in Fig. 10 in the case of coupled [curve (*a*)], and uncoupled [curve (*b*)] expansion.

The unregular oscillations observed in Fig. 8 can be ascribed to the sharp cut introduced by the condition on the interaction time depending on anharmonically oscillating terms. This suggests that a considerable improvement of the investigation can be obtained by reducing gas pressure steps.

A simple estimation of the threshold of the phenomenon can be carried out by comparing the coupling terms of Eqs. (12) with the respective time scales τ_j, at the end of the beam pulse, and by assuming that the f_e

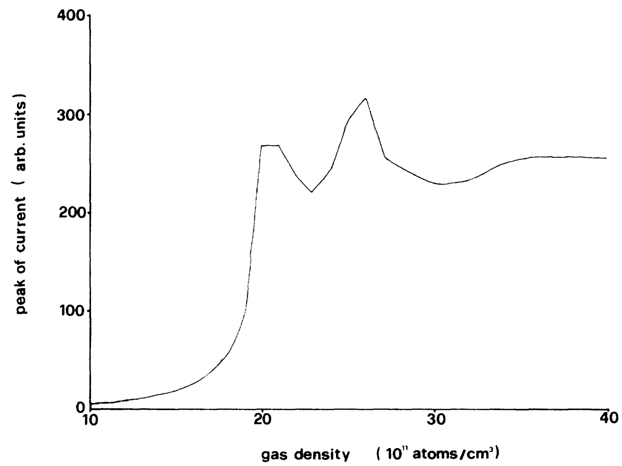

FIG. 8. Theoretical calculation of the dependence of the electron-current peak on gas density.

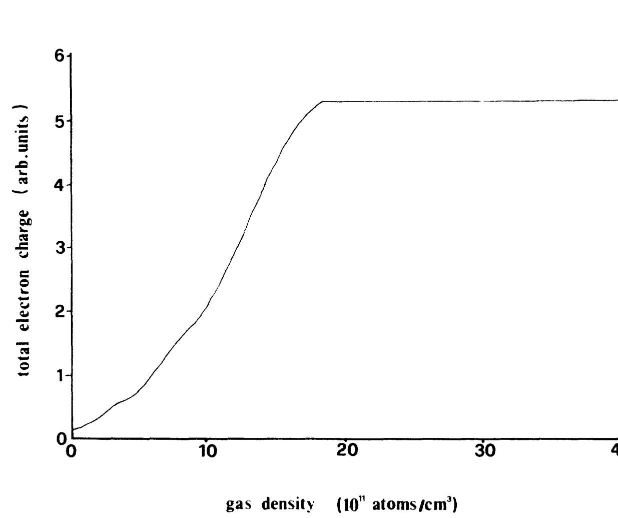

FIG. 9. Theoretically calculated dependence of the electron-current pulse total charge on the gas density.

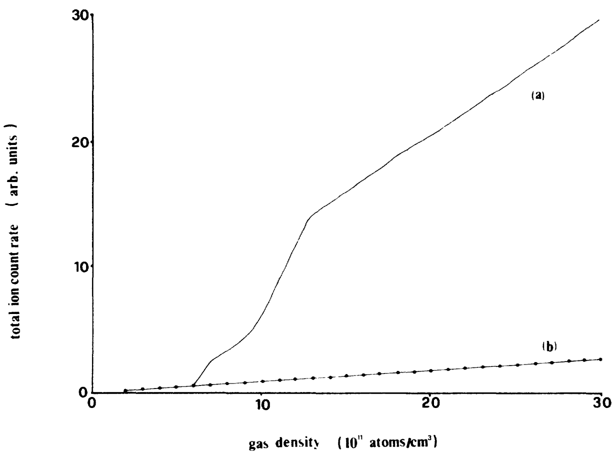

FIG. 10. Theoretical dependence of the total ion count rate as a function of the gas density in the case of coupled [curve (*a*)] and uncoupled [curve (*b*)] expansion of the charged species.

function of secondary electrons is negligible, owing to the fast expansion ($\tau_{se} \approx 0.1$ nsec), whereas f_i is close to 1 (ions are approximately at rest). In Eqs. (12), referred to the incident beam, the positive term inducing growth of the f_{px}, f_{pr} functions (focusing) is given by

$$(8\pi e^2/3m_e)Ng(t_{\rm int}) = (8\pi e^2/3m_e)N\langle a\rangle n_p t_{\rm int}$$

that, near the threshold of the phenomenon, is equal to the duration of the beam pulse (10 nsec), and $g(t)$ is simply given by $g(t) = \langle a\rangle n_p t$, owing to the low ionization rate. The negative terms depend on the electrostatic repulsion [$(8\pi e^2/3m_e)n_p$, with $f_{px} = f_{pr} = 1$] and on the random spread (τ_{px} and τ_{pr}). Thus, comparing positive and negative terms, the threshold condition is given by

$$N\langle a\rangle n_p t_{\rm int} \ge \frac{3E_B}{2\pi e^2 d_j^2} + n_p \ , \tag{16}$$

where E_B represents the energy spread of the beam, and the index j its radial or longitudinal width. By introducing the above data., Eq. (16) leads to a pressure value, for the threshold, of $\approx 3\times10^{-4}$ Torr. Considering that the actual pressure over the needle is about 100 times the background, this value is in a good agreement with the measured one ($\approx 10^{-3}$ Torr, see Figs. 2 and 3). It turns out from Eq. (16) that, in the case of negligible beam thermal spread (first term in the right-hand side less than n_p), as in the present experiment, the pressure threshold allows one to estimate the electron-impact ionization rate, i.e., $N \ge 1/\langle a\rangle t_0$.

In general, if the right-hand-side contribution in Eq. (16) is not negligible the radial and longitudinal thresholds, related respectively to the growth of total transmitted charge and to the peak value, could occur at different values of gas pressure.

In Eq. (10), relative to the ions, the terms responsible for the focusing are related to the density of primary and secondary electrons. During the interaction time and near or above the threshold, the density of secondary electrons decreases or oscillates around the value of the ion density, whereas the density of primary electrons suddenly increases. When $n_p f_{px}^{1/2} f_{pr}$ becomes greater than $Ng(t)$ (the ion thermal spread being negligible during the interaction time), the ion f_{si} function increases as an effect of the positive coupling term. Therefore, the ion focusing must occur in the same pressure range corresponding to the sudden growth of the incident beam density, i.e., transmitted current.

IV. COMPARISON WITH THE EXPERIMENTAL RESULTS

As Figs. 8–10 show, the main features of the phenomenon are reproduced by the above-mentioned approach. In particular, the sudden growth of the electron-beam current as well as the change of ion count rate slope in the same range of pressure are predicted. Moreover, the present analysis allows one to explain the different behavior observed when the gas fills, in a uniform way, the vacuum chamber. In that case the interaction region is only determined by the electron beam. This implies a reduction of two orders of magnitude of the characteristic time of the electron expansion rate (τ_{se}). As a consequence, during the interaction time the electron and ion profiles almost completely overlap and the focusing effect on the incident beam, produced by the electric field generated by their relative motion, disappears. Hence, as already pointed out, the appearance of the observed electron and ion focusing depends on the relative time scale of the involved physical effects. The authors of Refs. 14 and 15 observed similar phenomena at the beginning of the beam pulse but on a different time scale (≈ 2 μsec). In that case, in spite of the moderate density gradients, the effect appears, owing to the very long interaction time (some tenths of μsec).

In spite of the successful explanation of the main observed features, some disagreements arise in the quantitative comparison with the experimental results. As can be deduced from Figs. 8 and 9, the calculated ratios between maximum and minimum values of peak current and total charge are, respectively, about 100 and 30. The experimentally determined ratio for the total charge is in good agreement with the theoretical one, although the sudden increase of Fig. 3 [curve (*a*)] is steeper than in Fig. 9 and is observed at a slightly higher pressure ($\approx 2\times10^{-5}$ Torr). On the other hand, the experimental ratio for the peak current (≈ 10) differs by a factor of 10 from the calculated one. From the theoretical approach of Sec. III, it results that focusing effects along the radial and longitudinal directions produce different effects on the pulse temporal profile. Whereas the radial focusing enhances the peak value but does not affect the current profile; on the contrary, the longitudinal focusing essentially induces a reduction of the pulse duration. In fact, it results from the calculations that the pulse width in the plateau region is less than 0.1 nsec and continuously decreases, whereas the shortest experimental value was of about 2 nsec. A first rough explanation could invoke the bandpass of the electronic circuit to explain the reduced growth of the peak current. Moreover, while the behavior of peak current depends on both longitudinal and radial focusing effects the total charge signal is affected by the radial focusing only. Thus, the quantitative discrepancies between some features of the experimental and numerical results, such as the smoother growth of the theoretical curve of Fig. 9 and the absence of oscillations in the plateau region, can be ascribed to the oversimplified description of the beam radial divergence. In fact, in the theoretical approach the divergence of the beam after focusing in the interaction volume has not been considered.

Also in the case of the total ion count rate there is a satisfactory qualitative agreement between the experimental (Fig. 4) and numerical (Fig. 10) results. In particular, the theoretical approach is able to reproduce the two main features of our measurements: (i) the considerable increase in the total collected ionic charge (focusing effect) starting from a pressure of $\approx 1\times 10^{-5}$ Torr, when the gas sample is introduced through a needle injector [curves (*a*) of Figs. 4 and 10]; (ii) the absence of this focusing effect, at the same overall pressure, when the gas fills homogeneously the vacuum chamber (no needle injector) as shown by curve (*b*) of Fig. 4, and when in the theoretical calculation an uncoupled expansion is considered [curve (*b*) of Fig. 10]. We recall that the case of uncoupled expansion corresponds to a situation where, because of the low density of produced charges (low gas density), the self-induced electric field can be neglected.

V. DISCUSSION AND CONCLUSIONS

We have carried out an experimental analysis which highlights the presence of relevant collective effects, depending on electron-ion mutual interactions, in the ionization of a gas jet by impact with an incident monochromatic pulsed electron beam. The result of these collective plasma interactions is a noticeable focusing ion effect on the electronic beam, very similar to that already observed in Ref. 14, but at electron energies (≈ 40 eV) about 100 times smaller than those characterizing the beam of Refs. 14 and 15 (≈ 3 keV), and with an electron-beam–gas interaction time (≈ 10 nsec) that does not allow the establishment of a steady-state condition. In fact, this is the first time that the influence of collective effects is observed and analyzed in the experimental conditions characterizing the EI ionization of low-density atomic and molecular gases (pressure $\approx 10^{-5}$ Torr). In particular, in our experimental condition the focusing effect results in an increase of the axial current as measured by an electron detector whose radius is smaller than the radial width of the umperturbed electron beam, which monitors the electron current after it has passed through the target gas.

The observed effect shows a strong, threshold dependence on the gas pressure, i.e., on the degree of ionization produced, as clearly shown by curves (*a*) of Figs. 2 and 3. In particular, when the needle injector, which causes a local pressure about 100 times higher than the overall pressure, is eliminated and the vacuum chamber is uniformly filled at the same overall pressure, the effect disappears [curves (*b*) of Figs. 2 and 3].

Similar effects are also observed in the collected total ionic current (see Fig. 4). In fact, the efficiency of collection is enhanced by the ion focusing during the interaction with the incident electron beam. Moreover, the shape of the ionic peaks in the TOF spectrum is significantly distorted, as shown in the difference spectrum of Fig. 7, if compared to what is observed in the gas pressure range where the focusing effects do not occur. In particular, a relevant tail in the region of longer TOF's is present. The consequent broadening of the ionic peaks in the TOF mass spectrum can have important consequences in the field of mass analysis of gaseous samples, especially in the case of isotope separation of charged species.

We have also presented a simple theoretical model, based on the three-dimensional fluid description of the coupled motion of the involved charged species, which is able to reproduce, on a semiquantitative basis, the main features of the experiment. In particular, our theoretical approach gives a simple explanation of the thresholdlike behavior of the peak of the transmitted electron-beam current, and of the total ion count rate as a function of the gas pressure, as discussed at the end of Sec. IV. Moreover, a specific diagnostic of the internal features of this kind of plasma, e.g., the spectrum of electrostatic oscillations, should be added in order to improve our knowledge of the interaction phase that could constitute an important reference for the theoretical description of the time-space evolution of produced charges.

[1]F. Giammanco, Phys. Rev. A **36**, 5658 (1987).
[2]F. Giammanco, Phys. Rev. A **40**, 5160 (1989).
[3]F. Giammanco, Phys. Rev. A **40**, 5171 (1989).
[4]M. Crance, J. Phys. B **19**, L267 (1986).
[5]F. Yeargeau, G. Petite, and P. Agostini, J. Phys. B **19**, L663 (1986).
[6]G. Petite, P. Agostini, and F. Yeargeau, J. Opt. Soc. Am. B **4**, 765 (1987).
[7]L. A. Lompré, A. L'Huillier, G. Mainfray, and C. Manus, J. Opt. Soc. Am. B **2**, 1906 (1985).
[8]P. Kruit, J. Kimman, H. G. Muller, and M. J. van der Wiel, Phys. Rev. A **28**, 248 (1983).
[9]P. H. Bucksbaum, M. Bashkansky, R. R. Freeman, T. J. McIlrath, and L. F. DiMauro, Phys. Rev. Lett. **56**, 2590 (1986).
[10]T. J. McIlrath, P. H. Bucksbaum, R. R. Freeman, and M. Bashkansky, Phys. Rev. A **35**, 4611 (1987).
[11]B. Carré, F. Roussel, G. Spiess, J. M. Bizeau, P. Gerard, and F. Wuilleumier, Z. Phys. D **1**, 79 (1986).
[12]F. Roussel, B. Carré, P. Breger, and G. Spiess, J. Phys. B **14**, L313 (1981).
[13]For a review of the influence of "space-charge" phenomena in different field of investigation and involving mostly application see *Resonance Ionization Spectroscopy-III,* Institute of Physics Conference Series No. 84, edited by G. S. Hurst (Institute of Physics, Bristol, 1987); and *Resonance Ionization Spectroscopy-IV,* Institute of Physics Conference Series No.

94, edited by T. B. Lucatorto and J. E. Parks (Institute of Physics, Bristol, 1988).
[14]G. I. Guseva and M. A. Zav'yalov, Fiz. Plazmy **13**, 366 (1987) [Sov. J. Plasma Phys. **9** (4), 445 (1987)].
[15]V. P. Kovalenko and S. F. Fastovets, Fiz. Plazmy **9**, 964 (1983) [Sov. J. Plasma Phys. **9** (5), 562 (1983)].
[16]M. Armenante, V. Santoro, N. Spinelli, and F. Vanoli, Int. J. Mass Spectrom. Ion Proc. **64**, 265 (1985).
[17]G. Arena, M. Armenante, S. Salerni, and N. Spinelli, Rapid Commun. Mass Spectrom. **2**, 35 (1988).
[18]L. Spitzer, *Physics of Fully Ionized Gases* (Interscience, New York, 1956).
[19]C. W. Gear, *Numerical Initial Value Problems in Ordinary Differential Equations* (Englewood Cliffs, NJ, 1971).